11 Scale setting

Authors: R. Sommer, N. Tantalo, U. Wenger

Matching QCD to nature requires fixing the quark masses and matching an overall scale to experiment. That overall energy scale $\mathcal{S}$ may be taken, for example, as the nucleon mass. This process is referred to as scale setting.

11.1 Impact

The scale setting procedure, described in some detail below, is a rather technical step necessary to obtain predictions from QCD. What may easily be overlooked is that the exact predictions obtained from the theory, including many in this review, may depend rather sensitively on the scale.

As long as the theory is incomplete, e.g., because we have predictions from $N_f = 2 + 1$ QCD, results will depend on which physics scale is used. Whenever a theory scale (see Sec. 11.4) is used, it matters which value one imposes. Thus, to know whether computations of a particular quantity agree or not, one should check which (value for a) scale was used.

The sensitivity of predictions to the scale vary with the observable. For example, the Λ parameter of the theory has a linear dependence,

$$\frac{\delta\Lambda}{\Lambda} \approx \frac{\delta\mathcal{S}}{\mathcal{S}}\,, \tag{467}$$

because Λ has mass dimension one and other hidden dependencies on the scale are (usually) suppressed. Let us preview the results. The present precision on the most popular theory scale, w_0 in Eq. (503) is about 0.4% and for $\sqrt{t_0}$ it is 0.6%. On the Λ parameter it is about 3%. Thus, we would think that the scale uncertainty is irrelevant. However, in Sec. 11.7 we will discuss that differences between $N_f = 2 + 1$ and 2+1+1 numbers for $\sqrt{t_0}$ are at around 2%, which *does matter*.

Also, light-quark masses have an approximatively linear dependence on the scale (roughly speaking one determines, e.g., $m_{ud} = \frac{1}{\mathcal{S}} \times [M_\pi^2]_{\rm exp} \times [\frac{m_{ud}\mathcal{S}}{M_\pi^2}]_{\rm lat}$) and scale uncertainties may play an important rôle in the discussion of agreement vs. disagreement of computations within their error budget.

The list of quantities where scale setting is very important may be continued; we just want to mention an observable very much discussed at present, the hadronic vacuum-polarisation contribution to the anomalous magnetic moment of the muon [1]. It is easily seen that the dependence on the scale is about quadratic in that case [2],

$$\frac{\delta a_\mu^{\rm HVP}}{a_\mu^{\rm HVP}} \approx 2\frac{\delta\mathcal{S}}{\mathcal{S}}\,. \tag{468}$$

This fact means that scale setting has to be precise at the few per-mille precision for the $a_\mu^{\rm HVP}$ lattice determination to be relevant in the comparison with experiment.

11.2 Scale setting as part of hadronic renormalization schemes

We consider QCD with N_f quarks and without a θ-parameter. This theory is completely defined by its coupling constant as well as N_f quark masses. After these parameters are

specified all other properties of the theory are predictions. Coupling and quark masses depend on a renormalization scale μ as well as on a renormalization scheme. The most popular scheme in the framework of perturbative computations is the $\overline{\rm MS}$ scheme, but one may also define nonperturbative renormalization schemes, see Secs. 4 and 9.

In principle, a lattice computation may, therefore, use these $N_f + 1$ parameters as input together with the renormalization scale μ to fix the bare quark masses and coupling of the discretized Lagrangian, perform continuum and infinite-volume limit and obtain desired results, e.g., for decay rates.[1] However, there are various reasons why this strategy is inefficient. The most relevant one is that unless one uses lattice gauge theory to compute them, coupling and quark masses cannot be obtained from experiments without invoking perturbation theory and thus necessarily truncation errors. Moreover, these parameters are naturally short-distance quantities, since this is where perturbation theory applies. Lattice QCD on the other hand is most effective at long distances, where the lattice spacing plays a minor role. Therefore, it is more natural to proceed differently.

Namely, we may fix $N_f + 1$ nonperturbative, long-distance observables to have the values found in nature. An obvious choice are $N_f + 1$ hadron masses that are stable in the absence of weak interactions. This hadronic renormalization scheme is defined by

$$\frac{M_i(g_0, \{am_{0,\mathrm{j}}\})}{M_1(g_0, \{am_{0,\mathrm{j}}\})} = \frac{M_i^{\rm exp}}{M_1^{\rm exp}}\,, \quad i = 2 \ldots N_f + 1\,, \quad j = 1 \ldots N_f\,. \tag{469}$$

Here, M_i are the chosen hadron masses, g_0 is the bare coupling, and $am_{0,j}$ are the bare quark masses in lattice units. The ratio M_i/M_1 is, precisely speaking, defined through the hadron masses in lattice units, but in infinite volume. In QCD (without QED), all particles are massive. Therefore, the infinite volume limit of the properties of stable particles is approached with exponentially small corrections, which are assumed to be estimated reliably. The power-like finite-volume corrections in QCD+QED are discussed in Sec. 11.2.2. For fixed g_0, Eq. (469) needs to be solved for the bare quark masses,

$$am_{0,\mathrm{j}} = \mu_j(g_0)\,. \tag{470}$$

The functions μ_j define a line in the bare parameter space, called the line of constant physics. Its dependence on the set of masses $\{M_i\}$ is suppressed. The continuum limit is obtained as $g_0 \to 0$ with the lattice spacing shrinking roughly as $aM_1 \sim \mathrm{e}^{-1/(2b_0 g_0^2)}$. More precisely, consider observables $\mathcal{O}$ with mass dimension $d_{\mathcal{O}}$. One defines their dimensionless ratio

$$\hat{\mathcal{O}}(aM_1) = \left.\frac{\mathcal{O}}{M_1^{d_{\mathcal{O}}}}\right|_{am_{0,j}=\mu_j(g_0)}\,, \tag{471}$$

and obtains the continuum prediction as

$$\mathcal{O}^{\rm cont} = (M_1^{\rm exp})^{d_{\mathcal{O}}} \lim_{aM_1 \to 0} \hat{\mathcal{O}}(aM_1) \tag{472}$$

which explains why the determination and use of aM_1 is referred to as scale setting.

Equation (470) has to be obtained from numerical results. Therefore, it is easiest and most transparent if the i-th mass ratio depends predominantly on the i-th quark mass. Remaining for a while in the isospin-symmetric theory with $m_{0,1} = m_{0,2}$ (we enumerate the

[1] At first sight this seems like too many inputs, but note that it is the scale μ, at which $\alpha(\mu)$ has a particular value, which is the input. The coupling α by itself can have any (small) value as it runs.

quark masses in the order up, down, strange, charm, bottom and ignore the top quark), we have natural candidates for the numerators as the pseudoscalar masses in the associated flavour sectors, i.e., π, K, D, B. The desired strong dependence on light- (strange-)quark masses of π- (K-)meson masses derives from their pseudo-Goldstone nature of the approximate $\mathrm{SU(3)_L}\times\mathrm{SU(3)_R}$ symmetry of the massless QCD Lagrangian, which predicts that M_π^2 is roughly proportional to the light-quark mass and M_K^2 to the sum of light- and strange-quark masses. For D and B mesons approximate heavy-quark symmetry predicts M_D and M_B to be proportional to charm- and bottom-quark masses. Also other heavy-light bound states have this property. There is another important feature, which singles out pseudoscalar masses. Because they are the lightest particles with the given flavour quantum numbers, their correlation functions have the least signal/noise problem in the Monte Carlo evaluation of the path integral [3, 4].

Still restricting ourselves to isospin-symmetric QCD (isoQCD, see Sec. 3), we thus take it for granted that the choice M_i, $i \geq 2$ is easy, and we do not need to discuss it in detail: the pseudoscalar meson masses are very good choices, and some variations for heavy quarks may provide further improvements.

The choice of M_1 is more difficult. From the point of view of physics, a natural choice is the nucleon mass, $M_1 = M_\mathrm{nucl}$. Unfortunately it has a rather bad signal/noise problem when quark masses are close to their physical values. The ratio of signal to noise of the correlation function at time x_0 from N measurements behaves as [3]

$$R_{S/N}^\mathrm{nucl} \overset{x_0 \text{ large}}{\sim} \sqrt{N}\,\exp(-(M_\mathrm{nucl} - \frac{3}{2}M_\pi)\,x_0) \approx \sqrt{N}\,\exp(-x_0/0.27\,\mathrm{fm})\,, \tag{473}$$

where the numerical value of 0.27 fm uses the experimental masses. The behaviour in practice, but at still favourably large quark masses, is illustrated in Fig. 50. Because this property leads to large statistical errors and it is further difficult to control excited-state contaminations when statistical errors are large, it is useful to search for alternative physics scales. The community has gone this way, and we discuss some of them below. For illustration, here we just give one example: the decay constants of leptonic π or K decays have mass dimension one and can directly replace M_1 above. Figure 50 demonstrates their long and precise plateaux as a function of the Euclidean time. Advantages and disadvantages of this choice and others are discussed more systematically in Sec. 11.3.

11.2.1 Theory scales

Since the signal/noise problem of physics scales is rather severe, they were already replaced by theory scales in the very first days of lattice QCD. These scales cannot be determined from experiment alone. Rather, their values have to be computed by lattice QCD using a physics scale as input.

Creutz already used the string tension in his seminal paper on SU(2) Yang Mills theory [10], because it is far easier to determine than glueball masses. A further step was made by the potential scale r_0, defined in terms of the static force $F(r)$ as [11]

$$r_0^2 F(r_0) = 1.65\,. \tag{474}$$

Even though r_0 can vaguely be related to the phenomenology of charmonium and bottomonium states, its precise definition is in terms of $F(r)$ which can be obtained accurately from Monte Carlo lattice computations with (improvable) control over the uncertainties, but not

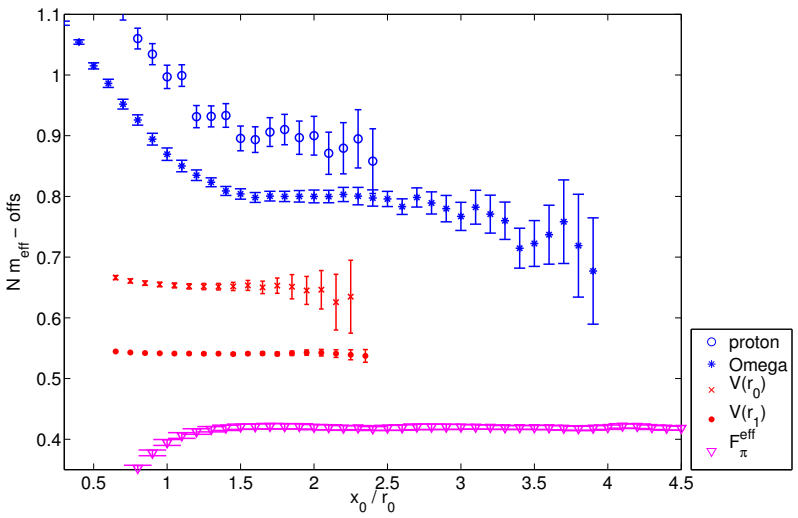

Figure 50: Effective masses for M_{proton} [5], M_Ω [6], $V(\approx r_0)$, $V(\approx r_1)$ [7] and f_π [8] on $N_f = 2$ CLS ensemble N6 with $a = 0.045\,\text{fm}$, $M_\pi = 340$ MeV on a $48^3 \times 96$ lattice [8]. All effective "masses" have been scaled such that the errors in the graph reflect directly the errors of the determined scales. They are shifted vertically by arbitrary amounts. Figure from Ref. [9]. Note that this example is at still favourably large quark masses. The situation for M_{proton} becomes worse closer to the physical point, but may be changed by algorithmic improvements.

from experiment. In that sense, it is a prototype of a theory scale.

Useful properties of a good theory scale are high statistical precision, easy to control systematics, e.g., weak volume dependence, quark-mass dependence only due to the fermion determinant, and low numerical cost for its evaluation. These properties are realized to varying degrees by the different theory scales covered in this section and, in this respect, they are much preferred compared to physics scales. Consequently, the physics scale M_1 has often been replaced by a theory scale as, e.g., $\mathcal{S} = r_0^{-1}$ in the form

$$\mathcal{O}^{\text{cont}} = \left(\mathcal{S}^{\text{phys}}\right)^{d_\mathcal{O}} \lim_{a\mathcal{S}\to 0} \hat{\mathcal{O}}_\mathcal{S}(a\mathcal{S}) \quad \text{with} \quad \hat{\mathcal{O}}_\mathcal{S}(a\mathcal{S}) = \left[\mathcal{S}^{-d_\mathcal{O}}\,\mathcal{O}\right]_{am_{0,j}=\mu_j(g_0)}\,, \tag{475}$$

and

$$\mathcal{S}^{\text{phys}} = (M_1^{\text{exp}}) \lim_{aM_1\to 0} \hat{\mathcal{S}}_{M_1}(aM_1)\,. \tag{476}$$

In this section, we review the determination of numerical results for the values of various theory scales in physical units, Eq. (476). The main difficulty is that a physics scale M_1 has to be determined first in order to connect to nature and, in particular, that the continuum limit of the theory scale in units of the physics scale has to be taken.

11.2.2 Isospin breaking

For simplicity and because it is a very good approximation, we have assumed above that all other interactions except for QCD can be ignored when hadron masses and many other

properties of hadrons are considered. This is a natural point of view because QCD is a renormalizable field theory and thus provides unique results.

However, we must be aware that while it is true that the predictions (e.g., for hadron masses M_i, $i > N_f + 1$) are unique once Eq. (469) is specified, they will change when we change the inputs $M_i^{\rm exp}$. These ambiguities are due to the neglected electroweak and gravitational interactions, namely because QCD is only an approximate—even if precise—theory of hadrons. At the sub-percent level, QED effects and isospin violations due to $m_u \neq m_d$ must be included. At that level one has a very precise description of nature, where weak decays or weak effects, in general, can be included perturbatively and systematically in an effective-field-theory description through the weak-effective-interaction Hamiltonian, while gravity may be ignored.

Scale setting is then part of the renormalization of QCD+QED, and in principle it is quite analogous to the previous discussion. Triviality of QED does not play a rôle at small enough α: we may think of replacing the continuum limit $a \to 0$ by a limit $a \to a_{\rm w}$ with $a_{\rm w}$ nonzero but very far below all physical QCD+QED scales treated. The definition and implementation of a hadronic renormalization scheme of QCD+QED defined on the lattice is discussed in Sec. 3. The electric charge appears as a new parameter and is conveniently fixed in the Thomson limit. Care needs to be taken in the separate definition of QED effects and strong isospin-breaking effects due to the up/down quark-mass difference. Here, we repeat Eq. (23),

$$X^\phi = \bar{X} + X_\gamma + X_{\rm SU(2)}\,, \tag{477}$$

and again emphasize that the split of physical observables X^ϕ into their isoQCD part, $\bar{X}$, the QED contributions, X_γ, and the strong IB effects, $X_{\rm SU(2)}$, is scheme dependent. In order to hopefully avoid confusion and to make it possible to average results also when they have a precision where the small IB-breaking effects matter, a particular scheme has been defined in Sec. 3. For quantities that enter in the averages, the schemes used in the computations are listed in Tab. 76. In this way, we can, to some degree, judge whether differences of results may also be due to the scheme used.

As a matter of fact, many existing lattice calculations have been performed in the isospin-symmetric limit, but not all the results considered in this review correspond to the very same definition of QCD. The different choices of experimental inputs are perfectly legitimate if QED radiative corrections are neglected, but in principle, predictions of isoQCD do depend on these choices, and it is not meaningful to average numbers obtained with different inputs. However, at the present level of precision the sub-percent differences in the inputs are most likely not relevant, and we will average and compare isoQCD results irrespective of these differences. The issue will become important when results become significantly more precise. Of course, the different inputs may not be ignored, when radiative corrections, Eq. (23), from various collaborations are directly compared. In this case, we strongly suggest to compare results for the unambiguous full theory observable or sticking to a standard.

11.3 Physical scales

The purpose of this short section is to summarize the most popular scales and give a short discussion of their advantages and disadvantages. We restrict ourselves to those used in more recent computations and, thus, the list is short.

Collaboration	Ref.	N_f	M_K [MeV]	scale	scale [MeV]
ETM 21	[12]	2+1+1	494.2	f_π	130.4
CalLat 20A	[13]	2+1+1	494.2	M_Ω	1672.5
MILC 15	[14]	2+1+1	494.5	$F_{p4s}(f_\pi)$	$153.90(9)(^{+21}_{-28})$
HPQCD 13A	[15]	2+1+1	494.6	f_π	130.4
Hudspith 24	[16]	2+1	494.2	M_Ω	1672.5
RQCD 22	[17]	2+1	494.2	M_Ξ	1316.9
CLS 21	[18]	2+1	497.6	$\frac{1}{3}(f_\pi + 2f_K)$	148.3
CLS 16	[19]	2+1	494.2	$\frac{1}{3}(f_\pi + 2f_K)$	147.6
RBC/UKQCD 14B	[20]	2+1	495.7	M_Ω	1672.5
HotQCD 14	[21]	2+1	n/a #	$r_1(f_\pi)$	0.3106 fm
BMW 12A	[22]	2+1	494.2	M_Ω	1672.5
Edinburgh consensus			494.6	f_π	130.5

The scheme uses $M_{\eta_{s\bar{s}}} \approx 695$ MeV instead of fixing $M_{\rm K}$.

Table 76: isoQCD schemes used in different computations as well as the Edinburgh consensus (see Sec. 3). We do not list the choice for M_π. It is $M_\pi = 135.0$ MeV throughout. As all quantities refer to the light sector of QCD only, charm quarks only enter through sea-quark effects. We therefore do not list which quantity is used to fix the charm-quark mass at the present stage.

11.3.1 The mass of the Ω baryon

As already discussed, masses of hadrons that are stable in QCD+QED and have a small width, in general, are very good candidates for physical scales since there are no QED infrared divergences to be discussed. Furthermore, remaining within this class, the radiative corrections are expected to be small. Furthermore, the Ω baryon has a significantly better noise/signal ratio than the nucleon (see Fig. 50). It also has little dependence on up- and down-quark masses, since it is composed entirely of strange valence quarks.

Still, one has to be aware that the mass is not extracted from the plateau region but from a modelling of the approach to a plateau in the form of fits [13, 20, 22–25]. In this sense, the noise/signal ratio problem may persist. The use of various interpolating fields for the Ω helps in constraining such analyses, but it would be desirable to have a theoretical understanding of multi-hadron (or in QCD+QED multi-hadron + photon) contributions as for the nucleon [26] discussed in Sec. 10. In the present review, we take the estimates of the collaborations at face value and do not try to apply a rating or an estimate of systematic error due to excited-state contributions.

11.3.2 Pion and kaon leptonic decay rates

These decay rates play a prominent rôle in scale setting, in (pure) QCD because excited-state contaminations can simply be avoided by going to sufficiently large Euclidean time. As a downside, QED radiative corrections need to be taken into account in the values assigned to the associated decay constants. Therefore, we briefly summarize the knowledge of QED radiative corrections and the definition of decay constants. More details are found in the previous edition of this review.

The physical observable is the decay rate $\Gamma^{\rm QCD+QED}[\pi^- \mapsto \mu\bar{\nu}_\mu(\gamma), E_\gamma]$ of a pion at rest.

It depends on the maximum energy E_γ of photons emitted in the decay and registered in the experimental measurement. These soft and hard photons can't be avoided since the cross-section vanishes as $E_\gamma \to 0$ and, e.g., the fixed-order cross-section without final-state photons is infrared divergent. However, apart from the dependence on E_γ, there are no ambiguities in the definition of $\Gamma^{\rm QCD+QED}$.

In QCD, the leptonic decay rate is,

$$\Gamma^{\rm QCD}[\pi \mapsto \mu\bar{\nu}_\mu] = \frac{G_F^2}{8\pi}|V_{ud}|^2\, M_{\pi^-}^{\rm exp}\left(m_\mu^{\rm exp}\right)^2\left[1-\frac{\left(m_\mu^{\rm exp}\right)^2}{\left(M_{\pi^-}^{\rm exp}\right)^2}\right]\left(f_\pi^{\rm QCD}\right)^2\,, \tag{478}$$

where one naturally introduces the decay constant,

$$f_\pi^{\rm QCD} = \frac{\langle 0|\,\bar{u}\gamma^0\gamma^5 d\,|\pi\rangle^{\rm QCD}}{M_\pi^{\rm QCD}}\,. \tag{479}$$

of the pion. Radiative corrections to $f_\pi^{\rm QCD}$ are then defined by

$$\delta f_\pi^{\rm QCD}(E_\gamma) = \sqrt{\frac{\Gamma^{\rm QCD+QED}[\pi^- \mapsto \mu\bar{\nu}_\mu(\gamma), E_\gamma]}{\Gamma^{\rm QCD}[\pi \mapsto \mu\bar{\nu}_\mu]}} - 1\,, \tag{480}$$

such that

$$\Gamma^{\rm QCD+QED}[\pi^- \mapsto \mu\bar{\nu}_\mu(\gamma), E_\gamma] = \Gamma^{\rm QCD}[\pi \mapsto \mu\bar{\nu}_\mu]\left[1+\delta f_\pi^{\rm QCD}(E_\gamma)\right]^2\,. \tag{481}$$

Common practice is to set

$$E_\gamma = E_\gamma^{\rm max} = \frac{M_{\pi^-}^{\rm exp}}{2}\left[1-\frac{\left(m_\mu^{\rm exp}\right)^2}{\left(M_{\pi^-}^{\rm exp}\right)^2}\right]\,, \tag{482}$$

the maximum energy allowed for a single photon in the case of negligible $\mathcal{O}(\alpha_{\rm em}^2)$ corrections.

As discussed in Sec. 3, $\delta f_\pi^{\rm QCD}(E_\gamma)$ depends on the scheme used to define QCD. However, the RM123 lattice determination in the electro-quenched approximation [27] found the scheme dependence to be irrelevant at the level of their result, $\delta f_\pi^{\rm isoQCD}(E_\gamma^{\rm max}) = 0.0076(9)$.[2] Additionally this agrees well with the estimate, $\delta f_\pi^{\rm isoQCD}(E_\gamma^{\rm max}) = 0.0088(11)$ from ChPT [28–30]. Taking V_{ud} from the PDG [31] (beta decays) and the ChPT number for δf_π, one has

$$f_\pi^{\rm isoQCD} = 130.56(2)_{\rm exp}(13)_{\rm QED}(2)_{V_{ud}}\,{\rm MeV}\,.$$

With the Edinburgh consensus Sec. 3, the scale of isoQCD is *defined* by

$$f_\pi^{\rm isoQCD} \equiv 130.5\,{\rm MeV}\,. \tag{483}$$

At the present level of accuracy the difference between the determined value (with a scheme uncertainty of around 1 permille) and the defining value (483) is irrelevant.

Some scale determinations use also the Kaon decay constant. There the understanding of QED radiative corrections is not yet as good as for pion decays. The ChPT estimate is

[2] More precisely, both a hadronic scheme and a so-called GRS scheme were tested, where as a simplification one may replace constant $\alpha_s(\mu_{\rm ref})$ across theories by constant lattice spacing in the electro-quenched approximation.

$\delta f_K^{\rm isoQCD}(E_\gamma^{\rm max}) = 0.0053(11)$ [28–30], while the electro-quenched lattice computation yielded $\delta f_K^{\rm isoQCD}(E_\gamma^{\rm max}) = 0.0012(5)$ [27]. As a slight update of the previous review, here we opt for a more conservative number of

$$\delta f_K^{\rm isoQCD}(E_\gamma^{\rm max}) = 0.003(3)\,, \tag{484}$$

encompassing both estimates. Together with $V_{us} = 0.2232(6)$ from Sec. 5 ($f_+(0)$ for $N_f = 2+1+1$) and the PDG decay rate, we have

$$f_K^{\rm isoQCD} = 157.4(2)_{\rm exp}(4)_{\rm QED}(4)_{V_{us}}\,\text{MeV}\,. \tag{485}$$

Depending on the lattice formulation, there is also a nontrivial renormalization of the axial current. Since it is easily determined from a chiral Ward identity, it does not play an important rôle. When it is present, it is assumed to be accounted for in the statistical errors.

11.3.3 Other physics scales

Scales derived from bottomonium have been used in the past, in particular, the splitting $\Delta M_\Upsilon = M_{\Upsilon(2s)} - M_{\Upsilon(1s)}$. They have very little dependence on the light-quark masses, but need an input for the b-quark mass. In all relevant cases, the b quark is treated by NRQCD.

11.4 Theory scales

In the following, we consider in more detail the two classes of theory scales that are most commonly used in typical lattice computations. The first class consists of scales related to the static quark-antiquark potential [11]. The second class is related to the action density renormalized through the gradient flow [32].

11.4.1 Potential scales

In this approach, lattice scales are derived from the properties of the static quark-antiquark potential. In particular, a scale can be defined by fixing the force $F(r)$ between a static quark and antiquark separated by the distance r in physical units [11]. Advantages of using the potential include the ease and accuracy of its computation, and its mild dependence on the valence-quark mass. In general, a potential scale r_c can be fixed through the condition that the static force takes a predescribed value, i.e.,

$$r_c^2 F(r_c) = X_c\,, \tag{486}$$

where X_c is a suitably chosen number. Phenomenological and computational considerations suggest that the optimal choice for X_c is in the region where the static force turns over from Coulomb-like to linear behaviour and before string breaking occurs. In the original work [11], it was suggested to use $X_0 = 1.65$ leading to the condition

$$r_0^2 F(r_0) = 1.65\,. \tag{487}$$

In Ref. [33], the value $X_1 = 1.0$ was proposed yielding the scale r_1.

The static force is the derivative of the static quark-antiquark potential $V(r)$ which can be determined through the calculation of Wilson loops. More specifically, the potential at

distance r is extracted from the asymptotic time dependence of the $r \times t$-sized Wilson loops $W(r,t)$,

$$V(r) = -\lim_{t\to\infty} \frac{d}{dt} \log\langle W(r,t)\rangle \,. \tag{488}$$

The derivative of the potential needed for the force is then determined through the derivative of a suitable local parameterization of the potential as a function of r, e.g.,

$$V(r) = C_- \frac{1}{r} + C_0 + C_+ r \,, \tag{489}$$

and estimating uncertainties due to the parameterization. In some calculations, the gauge field is fixed to Coulomb or temporal gauge in order to ease the computation of the potential at arbitrary distances.

In order to optimize the overlap of the Wilson loops with the ground state of the potential, one can use different types and levels of spatial gauge-field smearing and extract the ground-state energy from the corresponding correlation matrix by solving a generalized eigenvalue problem [34–36]. Finally, one can also make use of the noise reduction proposed in Refs. [37, 38]. It includes a smearing of the temporal parallel transporter [39] in the lattice definition of the discretized loops and thus yields a different discretization of the continuum force.

11.4.2 Gradient flow scales

The gradient flow $B_\mu(t,x)$ of gauge fields is defined in the continuum by the flow equation

$$\dot{B}_\mu = D_\nu G_{\nu\mu}, \quad B_\mu|_{t=0} = A_\mu \,, \tag{490}$$

$$G_{\mu\nu} = \partial_\mu B_\nu - \partial_\nu B_\mu + [B_\mu, B_\nu], \quad D_\mu = \partial_\mu + [B_\mu, \cdot\,] \,, \tag{491}$$

where A_μ is the fundamental gauge field, $G_{\mu\nu}$ the field-strength tensor, and D_μ the covariant derivative [32]. At finite lattice spacing, a possible form of Eqs. (490) and (491) is

$$a^2 \frac{d}{dt} V_t(x,\mu) = -g_0^2 \cdot \partial_{x,\mu} S_G(V_t) \cdot V_t(x,\mu) \,, \tag{492}$$

where $V_t(x,\mu)$ is the flow of the original gauge field $U(x,\mu)$ at flow time t, S_G is an arbitrary lattice discretization of the gauge action, and $\partial_{x,\mu}$ denotes the su(3)-valued differential operator with respect to $V_t(x,\mu)$. An important point to note is that the flow time t has the dimension of a length squared, i.e., $t \sim a^2$, and hence provides a means for setting the scale.

One crucial property of the gradient flow is that any function of the gauge fields evaluated at flow times $t > 0$ is renormalized [40] by just renormalizing the gauge coupling. Therefore, one can define a scale by keeping a suitable gluonic observable defined at constant flow time t, e.g., the action density $E = -\frac{1}{2}\operatorname{Tr} G_{\mu\nu}G_{\mu\nu}$ [32], fixed in physical units. This can, for example, be achieved through the condition

$$t_c^2 \langle E(t_c,x)\rangle = c \,, \quad E(t,x) = -\frac{1}{2}\operatorname{Tr} G_{\mu\nu}(t,x) G_{\mu\nu}(t,x) \,, \tag{493}$$

where $G_{\mu\nu}(t,x)$ is the field-strength tensor evaluated on the flowed gauge field V_t. Then, the lattice scale a can be determined from the dimensionless flow time in lattice units, $\hat{t}_c = a^2 t_c$. The original proposal in [32] was to use $c = 0.3$ yielding the scale t_0,

$$t_0^2 \langle E(t_0)\rangle = 0.3 \,. \tag{494}$$

For convenience one sometimes also defines $s_0 = \sqrt{t_0}$.

An alternative scale w_0 has been introduced in Ref. [22]. It is defined by fixing a suitable derivative of the action density,

$$W(t_c) = t_c \cdot \partial_t \left(t^2 \langle E(t) \rangle\right)_{t=t_c} = c\,. \tag{495}$$

Setting $c = 0.3$ yields the scale w_0 through

$$W(w_0^2) = 0.3\,. \tag{496}$$

In addition to the lattice scales from t_0 and w_0, one can also consider the scale from the dimensionful combination t_0/w_0. This combination is observed to have a very weak dependence on the quark mass [12, 41, 42].

A useful property of the gradient-flow scales is the fact that their quark-mass dependence is known from χPT [43].

Since the action density at $t \sim t_0 \sim w_0^2$ usually suffers from large autocorrelation [41, 44], the calculation of the statistical error needs special care.

Lattice artefacts in the gradient-flow scales originate from different sources [45], which are systematically discussed by considering t as a coordinate in a fifth dimension. First, there is the choice of the action S_G for $t > 0$. Second, there is the discretization of $E(t, x)$. Third, due to the discretization of the four-dimensional quantum action, and fourth, contributions of terms localized at the boundary $t = 0_+$. The interplay between the different sources of lattice artefacts turns out to be rather subtle [45].

Removing discretization errors due to the first two sources requires only classical (g_0-independent) improvement. Those due to the quantum action are common to all $t = 0$ observables, but the effects of the boundary terms are not easily removed in practice. At tree level, the Zeuthen flow [45] removes these effects completely, but none of the computations reviewed here have used it. Discretization effects due to S_G can be removed by using an improved action such as the tree-level Symanzik-improved gauge action [22, 46]. More phenomenological attempts of improving the gradient-flow scales consist of applying a t-shift [47], or tree-level improvement [48].

11.4.3 Other theory scales

The MILC collaboration has been using another set of scales, the partially-quenched pseudoscalar decay constant f_{p4s} with degenerate valence quarks with a mass $m_q = 0.4 \cdot m_{\text{strange}}$, and the corresponding partially quenched pseudoscalar mass M_{p4s}. So far it has been a quantity only used by the MILC collaboration [49–51]. We do not perform an in-depth discussion or an average but will list numbers in the results section.

Yet another scale that has been used is the leptonic decay constant of the η_s. This fictitious particle is a pseudoscalar made of a valence quark-antiquark pair with different (fictitious) flavours which are mass-degenerate with the strange quark [52–54].

11.5 List of computations and results

11.5.1 Gradient-flow scales

We now turn to a review of the calculations of the gradient-flow scales $\sqrt{t_0}$ and w_0. The results are compiled in Tab. 77 and shown in Fig. 51. In the following, we briefly discuss the calculations in the order that they appear in the table and figure.

Collaboration	Ref.	N_f	publication status	chiral extrapolation	continuum extrapolation	finite volume	physical scale	$\sqrt{t_0}$ [fm]	w_0 [fm]
ETM 21	[12]	2+1+1	A	★	★	★	f_π	0.14436(61)	0.17383(63)
CalLat 20A	[13]	2+1+1	A	★	★	★	M_Ω	0.1422(14)	0.1709(11)
BMW 20	[23]	1+1+1+1	A	★	★	★	M_Ω		0.17236(29)(63)[70]
ETM 20	[1076]	2+1+1	C	★	★	★	f_π		0.1706(18)
MILC 15	[14]	2+1+1	A	★	★	★	$F_{p4s}(f_\pi)^\#$	0.1416(+8/-5)	0.1714(+15/-12)
HPQCD 13A	[15]	2+1+1	A	★	○	★	f_π	0.1420(8)	0.1715(9)
Hudspith 24	[16]	2+1	P	★	★	★	$^\&$	0.14480(32)(6)	
RQCD 22	[17]	2+1	A	★	★	★	M_Ξ	0.1449(+7/-9)	
CLS 21	[18]	2+1	C	★	★	★	f_π, f_K	0.1443(7)(13)	
CLS 16	[19]	2+1	A	○	★	★	f_π, f_K	0.1467(14)(7)	
QCDSF/UKQCD 15B	[56]	2+1	P	○	○	○	$M_P^{\mathrm{SU}(3)}$	0.1511(22)(6)(5)(3)	0.1808(23)(5)(6)(4)
RBC/UKQCD 14B	[20]	2+1	A	★	★	★	M_Ω	0.14389(81)	0.17250(91)
HotQCD 14	[21]	2+1	A	★	★	★	$r_1(f_\pi)^\#$		0.1749(14)
BMW 12A	[22]	2+1	A	★	★	★	M_Ω	0.1465(21)(13)	0.1755(18)(4)

$^\#$ These scales are not physical scales and have been determined from f_π.
$^\&$ There is no physical scale as such. The input is the quark-mass dependence of M_Ω.

Table 77: Results for gradient flow scales at the physical point, cf. Eq. (476). Note that BMW 20 [23] take IB and QED corrections into account. An additional result for the ratio of scales is:
ETM 21 [12]: $t_0/w_0 = 0.11969(62)$ fm.

ETM 21 [12] finalizes and supersedes ETM 20 discussed below. It determines the scales $\sqrt{t_0}, w_0$, also $t_0/w_0 = 0.11969(62)$ fm, and the ratio $\sqrt{t_0}/w_0 = 0.82930(65)$, cf. also HPQCD 13A [15]. Since ETM 21 is now published, the values replace the ones of ETM 20 in the previous FLAG average.

CalLat 20A [13] use Möbius Domain-Wall valence fermions on HISQ ensembles generated by the MILC and CalLat collaborations. The gauge fields entering the Möbius Domain-Wall operator are gradient-flow smeared with $t = a^2$. They compute the Ω mass and the scales w_0, t_0 and perform global fits to determine $w_0 M_\Omega$ and $\sqrt{t_0} M_\Omega$ at the physical point. The flow is discretized with the Symanzik tree-level improved action and the clover discretization of $E(t)$ is used. A global fit with Bayesian priors is performed including terms derived from χPT for finite-volume and quark-mass dependencies, as well as a^2 and $a^2\alpha_s(1.5/a)$ terms for discretization errors. Also, a tree-level improved definition of the GF scales is used where the leading-in-g^2 cutoff effects are removed up to and including $\mathcal{O}(a^8/t^4)$.

BMW 20 [23] presents a result for w_0 in the context of their staggered-fermion calculation of the muon anomalous magnetic moment. It is the first computation that takes QED and isospin-breaking corrections into account. The simulations are performed by using staggered fermions with stout gauge-field smearing with six lattice spacings and several pion masses around the physical point with M_π between 110 and 140 MeV. Volumes are around $L = 6$ fm. At the largest lattice spacing, it is demonstrated how the effective masses of the Ω correlator almost reach the plateau value extracted from a four-state fit (two states per parity). Within

the range where the data are fit, the deviation of data points from the estimated plateau is less than a percent. Isospin-breaking corrections are computed by Taylor expansion around isoQCD with QED treated as $\mathrm{QED_L}$ [57]. Finite-volume effects in QED are taken from the $1/L, 1/L^2$ universal corrections and $\mathcal{O}(1/L^3)$ effects are neglected. The results for $M_\Omega w_0$ are extrapolated to the continuum by a fit with a^2 and a^4 terms.

ETM 20 [1076] presents in their proceedings contribution a preliminary analysis of their $N_f = 2+1+1$ Wilson twisted-mass fermion simulations at maximal twist (i.e., automatic $\mathcal{O}(a)$ improved), at three lattice spacings and pion masses at the physical point. Their determination of $w_0 = 0.1706(18)$ fm from f_π using an analysis in terms of M_π is the value quoted above. They obtain the consistent value $w_0 = 0.1703(18)$ fm from an analysis in terms of the renormalized light quark mass.

MILC 15 [14] sets the physical scale using the fictitious pseudoscalar decay constant $F_{p4s} = 153.90(9)(+21/-28)$ MeV with degenerate valence quarks of mass $m_v = 0.4m_s$ and physical sea-quark masses [51]. (F_{p4s} has strong dependence on the valence-quark mass and is determined from f_π.) They use a definition of the flow scales where the tree-level lattice artefacts up to $\mathcal{O}(a^4/t^2)$ are divided out. Charm-quark mass mistunings are between 1% and 11%. They are taken into account at leading order in $1/m_c$ through $\Lambda^{(3)}_{\mathrm{QCD}}$ applied directly to F_{p4s} and $1/m_c$ corrections are included as terms in the fits. They use elaborate variations of fits in order to estimate extrapolation errors (both in GF scales and F_{p4s}). They include errors from FV effects and experimental errors in f_π in F_{p4s}.

HPQCD 13A [15] uses eight MILC-HISQ ensembles with lattice spacings $a = 0.088$, 0.121, 0.151 fm. Values of L are between 2.5 fm and 5.8 fm with $M_\pi L = 3.3$–4.6. Pion masses range between 128 and 306 MeV. QCD is defined by using the inputs $M_\pi = 134.98(32)$ MeV, $M_K = 494.6(3)$ MeV, $f_{\pi^+} = 130.4(2)$ MeV derived by model subtractions of IB effects. Additional scale ratios are given: $\sqrt{t_0}/w_0 = 0.835(8)$, $r_1/w_0 = 1.789(26)$.

Hudspith 24 [16] computes the mass of the Omega baryon on CLS $N_f = 2{+}1$ configurations along the trajectories with approximately constant trace of the bare quark-mass matrix. They use 27 ensembles with six different values of the lattice spacing from $a = 0.09$ fm to $a = 0.04$ fm. They compute the (nonpositive) correlation function $C_\Omega(x_0)$ of a local field with a gauge-fixed wall-source, which results in a very good statistical precision. It is analyzed directly with a two-state fit describing the data over a large range. In addition they also extract M_Ω by constructing a 2x2 generalized Pencil-of-Functions matrix correlator from $C_\Omega(x_0)$, $C_\Omega(x_0+a)$, $C_\Omega(x_0+2a)$. Projecting with a GEVP eigenvector (from a fixed-time GEVP) a correlation function with a long plateau of the effective mass is found. Precisions for the Omega mass on various ensembles range from a few per mille to below a per mille. These masses, together with the scale t_0 are subsequently fit using a phenomenology- and ChPT-motivated form where a few parameters are taken from previous ChPT fits [58] to baryon masses computed on CLS ensembles by RQCD [17]. The dependence on t_0 is in the higher-order chiral-correction terms which include NNNLO. There is no term in the fit which allows for discretization effects in the chiral corrections. Their absence is justified by the results of previous fits in [58]. Given the unconventional analysis carried out in this work, the WG hopes that additional technical information will be provided in the published version of the paper (in particular concerning the direction in parameter space of the global fit of the Ω, kaon and pion masses from which the continuum value of t_0 is extracted) and may reconsider the ★ assigned in this review, on the basis of the standard continuum-limit criterion, once the paper is published and eligible to enter the average. Once the precision for the raw values

of am_Ω is independently confirmed, this paper [16], possibly with a new analysis, may lead to very high-precision determinations of the theory scales.

RQCD 22 [17] is an independent analysis of CLS ensembles employing $N_f = 2 + 1$ non-perturbatively improved Wilson fermions and the tree-level Symanzik improved gauge action. It uses a multitude of quark-mass combinations at six different values of the lattice spacing, ranging from $a \lesssim 0.098$ fm down to $a < 0.039$ fm. Near-physical quark masses are realized at $a = 0.064$ fm and $a = 0.085$ fm. The input quantities used to fix the physical point and to set the scale are $M_\pi = 134.8(3)$ MeV, $M_K = 494.2(3)$ MeV, and $m_\Xi = 1316.9(3)$ MeV (last line of pg. 33 in [17]). As RQCD 22 has been published since the last update, the result for $\sqrt{t_0}$ is now included in the FLAG average.

CLS 21 [18] is a proceedings contribution describing a preliminary analysis following the one in CLS 16 [19], cf. the description below. CLS 21 includes about twice the number of ensembles as compared to CLS 16, in particular, ensembles at two more lattice spacings and two ensembles at the physical point. As a consequence, this analysis is not considered a straightforward update and hence does not supersede the result of CLS 16.

CLS 16 [19] uses CLS configurations of 2+1 nonperturbatively $\mathcal{O}(a)$-improved Wilson fermions. There are a few pion masses with the strange mass adjusted along a line of $m_u + m_d + m_s = \text{const}$. Three different lattice spacings are used. They determine t_0 at the physical point defined by π and K masses and the linear combination $f_K + \frac{1}{2} f_\pi$. They use the Wilson flow with the clover definition of $E(t)$.

QCDSF 15B [56, 59] results, unpublished, are obtained by simulating $N_f = 2 + 1$ QCD with the tree-level Symanzik-improved gauge action and clover Wilson fermions with single-level stout smearing for the hopping terms together with unsmeared links for the clover term (SLiNC action). Simulations are performed at four different lattice spacings, in the range $[0.06, 0.08]$ fm, with $M_{\pi,\text{min}} = 228$ MeV and $M_{\pi,\text{min}} L = 4.1$. The results for the gradient-flow scales have been obtained by relying on the observation that flavour-symmetric quantities get corrections of $\mathcal{O}((\Delta m_q)^2)$ where Δm_q is the difference of the quark mass from the SU(3)-symmetric value. The $\mathcal{O}(\Delta m_q^2)$ terms are not detected in the data and subsequently neglected.

RBC/UKQCD 14B [20] presents results for $\sqrt{t_0}$ and w_0 obtained in QCD with $2 + 1$ dynamical flavours. The simulations are performed by using domain-wall fermions on six ensembles with lattice spacing $a^{-1} = 1.38, 1.73, 1.78, 2.36, 2.38$, and 3.15 GeV, pion masses in the range $M_\pi^{unitary} \in [139, 360]$ MeV. The simulated volumes are such that $M_\pi L > 3.9$. The effective masses of the Ω correlator are extracted with two-state fits and it is shown, by using two different nonlocal interpolating operators at the source, that the correlators almost reach a pleateau. In the calculation of $\sqrt{t_0}$ and w_0, the clover definition of $E(t)$ is used. The values given are $\sqrt{t_0} = 0.7292(41)\,\text{GeV}^{-1}$ and $w_0 = 0.8742(46)\,\text{GeV}^{-1}$ which we converted to the values in Tab. 77.

HotQCD 14 [21] determines the equation of state with $N_f = 2+1$ flavours using highly improved staggered quarks (HISQ/tree). As a byproduct, they update the results of HotQCD 11 [60] by adding simulations at four new values of β, for a total of 24 ensembles, with lattice spacings in the range $[0.04, 0.25]$ fm and volumes in the range $[2.6, 6.1]$ fm with $M_\pi = 160$ MeV. They obtain values for the scale parameters r_0 and w_0, via the ratios $r_0/r_1, w_0/r_1$ and using $r_1 = 0.3106(14)(8)(4)$ fm from MILC 10 [61]. They obtain for the ratios $(r_0/r_1)_{cont} = 1.5092(39)$ and $(w_0/r_1)_{cont} = 0.5619(21)$ in the continuum. They cross-check their determination of the scale r_1 using the hadronic quantities f_K, f_η from HPQCD 09B [53] and the experimental value of M_φ, and find good agreement.

BMW 12A [22] is the work in which w_0 was introduced. Simulations with 2HEX smeared

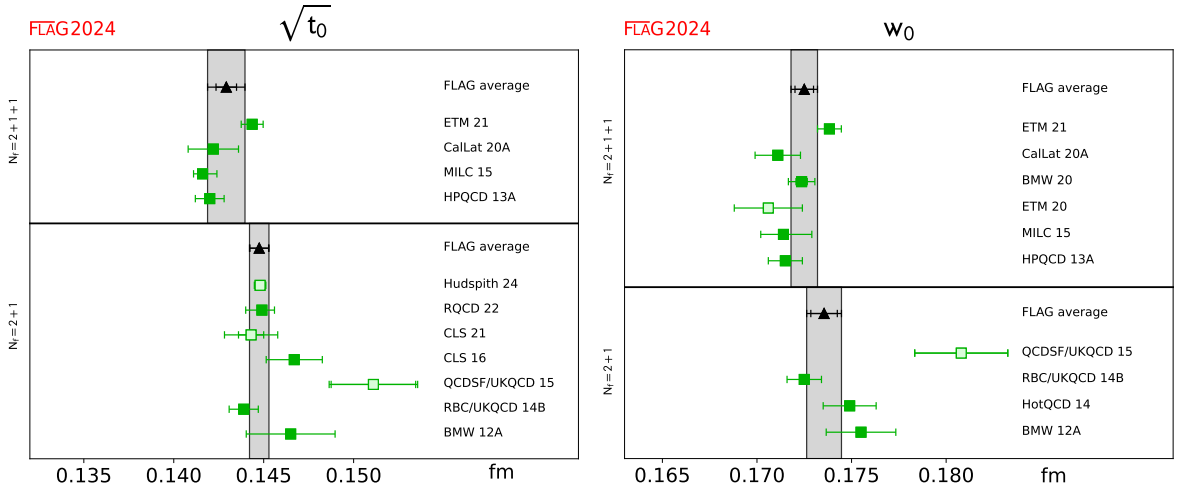

Figure 51: Results for gradient flow scales.

Wilson fermions and two-level stout-smeared rooted staggered fermions are done. The Wilson flow with clover $E(t)$ is used, and a test of the Symanzik flow is carried out. They take the results with Wilson fermions as their central value, because those "do not rely on the 'rooting' of the fermion determinant". Staggered fermion results agree within uncertainties.

11.5.2 Potential scales

We now turn to a review of the calculations of the potential scales r_0 and r_1. The results are compiled in Tab. 78 and shown in Fig. 52. With the exception of TUMQCD 22 [62], the most recent calculations date back to 2014, and we discuss them in the order that they appear in the table and the figure.

Asmussen 23 [64] perform a computation of the potential at five lattice spacings down to $a = 0.04$ fm on CLS ensembles. The ground-state level is extracted from a GEVP, starting from smeared Wilson loops with different levels of smearing. The results are thus far only available as a conference proceedings. The final result for r_0 originates from a global fit incorporating the pion-mass dependence and the lattice-spacing dependence.

TUMQCD 22 [62] uses HISQ ensembles generated by MILC at six lattice spacings ranging from $a = 0.15$ fm to $a = 0.03$ fm to compute the potential. Scale setting is performed through f_{p4s} [50]. In contrast to other determinations, the static potential is extracted using Coulomb-gauge fixing on two time-slices and the Wilson lines connecting the two time-slices. Thus, there is no variational method but fits are performed with up to three energy levels. Both continuum extrapolations with a^2 corrections and $\alpha^2(1/a)\,a^2$ are performed, where there is a preselection of the direction $\vec{r}/r$ and direction-dependent discretization effects are assumed to be sufficiently reduced by the use of the tree-level improved r_1 [11]. The final results come from a Bayesian model average.

ETM 14 [63] uses $N_f = 2 + 1 + 1$ Wilson twisted-mass fermions at maximal twist (i.e., automatic $\mathcal{O}(a)$-improved), three lattice spacings and pion masses reaching down to $M_\pi = 211$ MeV. They determine the scale r_0 through $f_\pi = f_{\pi^+} = 130.41$ MeV. A crosscheck of the so-obtained lattice spacings with the ones obtained via the fictitious pseudoscalar meson $M_{s's'}$ made of two strange-like quarks gives consistent results. The crosscheck is done using the

Collaboration	Ref.	N_f	publication status	chiral extrapolation	continuum extrapolation	finite volume	physical scale	r_0 [fm]	r_1 [fm]
TUMQCD 22	[62]	2+1+1	A	★	★	★	f_{p4s} ([50]) [$]	0.4547(64)	0.3037(25)
ETM 14	[63]	2+1+1	A	○	★	★	f_π	0.474(14)	
HPQCD 13A	[15]	2+1+1	A	★	○	★	f_π		0.3112(30)
HPQCD 11B	[52]	2+1+1	A	○	○	○	ΔM_Υ, f_{η_s}		0.3209(26)
Asmussen 23	[64]	2+1	C	★	★	★	f_π, f_K	0.4671(64)	
HotQCD 14	[21]	2+1	A	★	★	★	r_1([61]) [#]	0.4671(41)	
χQCD 14	[65]	2+1	A	○	○	○	three inputs[3]	0.465(4)(9)	
HotQCD 11	[60]	2+1	A	★	★	★	f_π	0.468(4)	
RBC/UKQCD 10A	[24]	2+1	A	○	○	○	M_Ω	0.487(9)	0.333(9)
MILC 10	[61]	2+1	C	○	★	★	f_π		0.3106(8)(14)(4)
MILC 09	[66]	2+1	A	○	★	★	f_π		$0.3108(15)(^{+26}_{-79})$
MILC 09A	[67]	2+1	C	○	★	★	f_π		$0.3117(6)(^{+12}_{-31})$
HPQCD 09B	[53]	2+1	A	○	★	○	three inputs		0.3133(23)(3)
PACS-CS 08	[25]	2+1	A	★	■	■	M_Ω	$0.4921(64)(^{+74}_{-2})$	
HPQCD 05B	[54]	2+1	A	○	○	○	ΔM_Υ	0.469(7)	0.321(5)
Aubin 04	[68]	2+1	A	○	○	○	ΔM_Υ	0.462(11)(4)	0.317(7)(3)

[#] This theory scale was determined in turn from r_1 [61].
[$] This theory scale was determined in turn from f_π.

Table 78: Results for potential scales at the physical point, cf. Eq. (476). $\Delta M_\Upsilon = M_{\Upsilon(2s)} - M_{\Upsilon(1s)}$.

dimensionless combinations $r_0 M_{s's'}$ (with r_0 in the chiral limit) and $f_\pi/M_{s's'}$ determined in the continuum, and then using r_0/a and the value of $M_{s's'}$ obtained from the experimental value of f_π. We also note that in Ref. [41] using the same ensembles the preliminary value $w_0 = 0.1782$ fm is determined, however, without error due to the missing or incomplete investigation of the systematic effects.

HPQCD 13A [15] was already discussed above in connection with the gradient flow scales.

HPQCD 11B [52] uses five MILC-HISQ ensembles and determines r_1 from $M_{\Upsilon(2s)} - M_{\Upsilon(1s)}$ and the decay constant f_{η_s} (see HPQCD 09B). The valence b quark is treated by NRQCD, while the light valence quarks have the HISQ discretization, identical to the sea quarks.

HotQCD 14 [21] was already discussed in connection with the gradient flow scales.

χQCD 14 [65] uses overlap fermions as valence quarks on $N_f = 2+1$ domain-wall fermion gauge configurations generated by the RBC/UKQCD collaboration [24]. Using the physical masses of D_s, D_s^* and J/ψ as inputs, the strange- and charm-quark masses and the decay contant f_{D_s} are determined as well as the scale r_0.

HotQCD 11 [60] uses configurations with tree-level improved Symanzik gauge action and HISQ staggered quarks in addition to previously generated ensembles with p4 and asqtad staggered quarks. In this calculation, QCD is defined by generating lines of constant physics with $m_l/m_s = \{0.2, 0.1, 0.05, 0.025\}$ and setting the strange-quark mass by requiring that the mass of a fictious $\eta_{s\bar{s}}$ meson is $M_{\eta_{s\bar{s}}} = \sqrt{2M_K^2 - M_\pi^2}$. The physical point is taken to be

at $m_l/m_s = 0.037$. The physical scale is set by using the value $r_1 = 0.3106(8)(18)(4)$ fm obtained in Ref. [61] by using f_π as physical input. In the paper, this result is shown to be consistent within the statistical and systematic errors with the choice of f_K as physical input. The result $r_0/r_1 = 1.508(5)$ is obtained by averaging over 12 ensembles at $m_l/m_s = 0.05$ with lattice spacings in the range $[0.066, 0.14]$ fm. This result is then used to get $r_0 = 0.468(4)$ fm. Finite-volume effects have been monitored with 20 ensembles in the range $[3.2, 6.1]$fm with $M_\pi L > 2.6$.

RBC/UKQCD 10A [24] uses $N_f = 2 + 1$ flavours of domain-wall quarks and the Iwasaki gauge action at two values of the lattice spacing with unitary pion masses in the approximate range $[290, 420]$ MeV. They use the masses of π and K meson and of the Ω baryon to determine the physical quark masses and the lattice spacings, and so obtain estimates of the scales r_0, r_1 and the ratio r_1/r_0 from a combined chiral and continuum extrapolation.

MILC 10 [61] presents a further update of r_1 with asqtad-staggered-quark ensembles with $a \in \{0.045, 0.06, 0.09\}$ fm. It supersedes MILC 09 [66, 67, 69].

MILC 09 [66] presents an $N_f = 2+1$ calculation of the potential scales on asqtad-staggered-quark ensembles with $a \in \{0.045, 0.06, 0.09, 0.12, 0.15, 0.18\}$ fm. The continuum extrapolation is performed by using Goldstone-boson pions as light as $M_\pi = 224$ MeV (RMS pion mass of 258 MeV). The physical scale is set from f_π. The result for r_1 obtained in the published paper [66] is then updated and, therefore, superseded by the conference proceedings MILC 09A and 09B [67, 69].

HPQCD 09B [53] is an extension of HPQCD 05B [54] and uses HISQ valence quarks instead of asqtad quarks. The scale r_1 is obtained from three different inputs. First $r_1 = 0.309(4)$ fm from the splitting of 2S and 1S Υ states as in Ref. [54], second $r_1 = 0.316(5)$ fm from $M_{D_s} - M_{\eta_s}/2$ and third $r_1 = 0.315(3)$ fm from the decay constant of the η_s. The ficitious η_s state is operationally defined by setting quark masses to the s-quark mass and dropping disconnected diagrams. Its mass and decay constant are obtained from a partially-quenched-chiral-perturbation-theory analysis using the pion and kaon states from experiment together with various partially-quenched lattice data. The three results are combined to $r_1 = 0.3133(23)(3)$ fm.

PACS-CS 08 [25] presents a calculation of r_0 in $N_f = 2 + 1$ QCD by using NP $\mathcal{O}(a)$-improved clover Wilson quarks and Iwasaki gauge action. The calculation is done at fixed lattice spacing $a = 0.09$ fm and is extrapolated to the physical point from (unitary) pion masses in the range $[156, 702]$ MeV. The $N_f = 2 + 1$ theory is defined by fixing M_π, M_K, and M_Ω to 135.0, 497.6, and 1672.25 MeV, respectively. The effective masses of smeared-local Ω correlators averaged over the four spin polarizations show quite good plateaux.

RBC/Bielefeld 07 [70] performed calculations of the equation of state with two light-quark flavours and a heavier strange quark using improved staggered fermions. Zero-temperature calculations including the static-quark potential were used to set the temperature scale for the thermodynamic observables. The lattice cut-off changes by a factor 6 from $a \simeq 0.3$ fm down to $a \simeq 0.05$ fm while the pion mass is kept fixed at $M_\pi \simeq 220(4)$ MeV. Apart from the dimensionless ratio $r_0/r_1 = 1.4636(60)$ they also provide a result for the ratio $r_0\sqrt{\sigma} = 1.1034(40)$

HPQCD 05B [54] performed the first bottomonium spectrum calculation in full QCD with $N_f = 2 + 1$ on MILC asqtad configurations and the b quark treated by NRQCD. They find agreement of the low lying Υ states with experiment and also compare to quenched and $N_f = 2$ results. They determined r_0 and r_1 from the splitting of 2S and 1S states.

Aubin 04 [68] presents an $N_f = 2 + 1$ calculation of the potential scales by using asqtad

staggered quark ensembles with $a = 0.09$ and $0.12\}$ fm. The continuum extrapolation is performed by using Goldstone-boson pions as light as $M_\pi = 250$ MeV. The physical scale is set from the Υ 2S-1S and 1P-1S splittings computed with NRQCD by HPQCD [71].

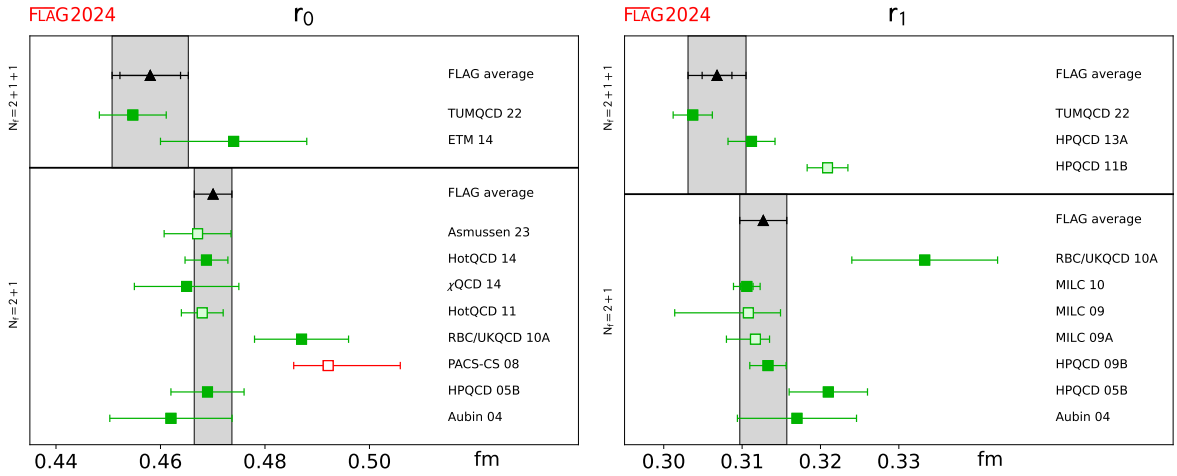

Figure 52: Results for potential scales.

11.5.3 Ratios of scales

It is convenient in many cases to also have ratios of scales at hand. In addition to translating from one scale to another, the ratios provide important crosschecks between different determinations. Results on ratios provided by the collaborations are compiled in Tab. 79 and Fig. 53. The details of the computations were already discussed in the previous sections.

Collaboration	Ref.	N_f	publication status	chiral extrapolation	continuum extrapolation	finite volume	$\sqrt{t_0}/w_0$	r_0/r_1	r_1/w_0
TUMQCD 22	[62]	2+1+1	A	★	★	★		1.4968(69)	
ETM 21	[12]	2+1+1	A	★	★	★	0.82930(65)		
HPQCD 13A	[15]	2+1+1	A	★	○	★	0.835(8)		1.789(26)
HotQCD 14	[21]	2+1	A	★	★	★			1.7797(67)
HotQCD 11	[60]	2+1	A	★	★	★		1.508(5)	
RBC/UKQCD 10A	[24]	2+1	A	○	○	○		1.462(32)[#]	
RBC/Bielefeld 07	[70]	2+1	A	■	★	★		1.4636(60)	
Aubin 04	[68]	2+1	A	○	○	○		1.474(7)(18)	

[#]This value is obtained from $r_1/r_0 = 0.684(15)(0)(0)$.

Table 79: Results for dimensionless ratios of scales.

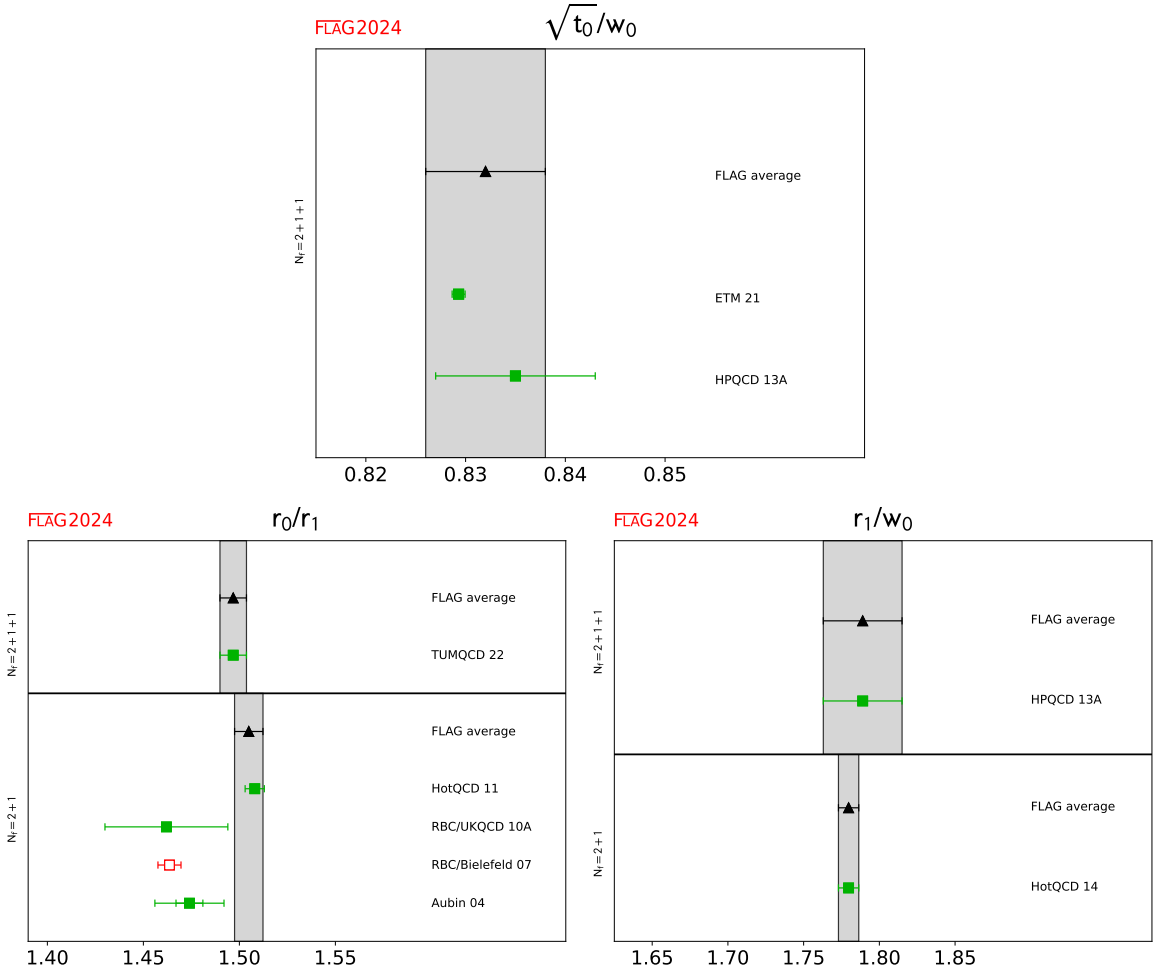

Figure 53: Results for dimensionless ratios of scales.

11.6 Averages

Data-driven continuum-limit criterion

As discussed in Sec. 2.1.2, we evaluate the inflation factor

$$s(a) = \max[1, 1 + 2(\delta(a) - 3)/3]\,, \quad \delta(a) = \frac{|Q(a) - Q(0)|}{\sigma_Q}\,, \tag{497}$$

where Q is the quantity for which we perform an average, and σ_Q is the uncertainty estimated by the collaboration for its continuum limit. If $s(a_{\rm min})$ exceeds one, i.e., if the continuum limit is more than three σ_Q from the result at smallest lattice spacing, $a_{\rm min}$, the error of the computation is inflated by $s(a_{\rm min})$ before taking the average. For our quantities $s(a_{\rm min}) = 1$ except for few cases. We therefore report explicitly values of $s(a_{\rm min})$ only where $s(a_{\rm min}) > 1$.

Gradient flow scale $\sqrt{t_0}$

For $N_f = 2+1+1$, we have two recent calculations from ETM 21 [12] and CalLat 20A [13], and two less recent ones from MILC 15 [14] and HPQCD 13A [15] fulfilling the FLAG criteria to enter the average. The latter two and CalLat 20A are based on the same MILC-HISQ gauge-field ensembles, hence we consider their statistical errors to be 100% correlated.

For $N_f = 2+1$, we have four calculations from RQCD 22 [17], CLS 16 [19], RBC/UKQCD 14B [20], and BMW 12A [22] which enter the FLAG average. RQCD 22 and CLS 16 are based on the same gauge-field ensembles, hence we consider their statistical errors to be 100% correlated. The other two are independent computations, so there is no correlation to be taken into account. QCDSF/UKQCD 15B [56] does not contribute to the average, because it is not published. CLS 21 [18] is a proceedings contribution based on double the number of ensembles. It is therefore not a straightforward update and does not supersede CLS 16 [19]. Performing the weighted and correlated average we obtain

$$N_f = 2+1+1: \qquad \sqrt{t_0} = 0.14292(104)\ \text{fm} \qquad \text{Refs. [12–15]}, \tag{498}$$

$$N_f = 2+1: \qquad \sqrt{t_0} = 0.14474(57)\ \text{fm} \qquad \text{Refs. [17, 19, 20, 22]}. \tag{499}$$

We note that the $N_f = 2+1+1$ results of staggered fermions and the twisted-mass result are not well compatible. The resulting stretching factor based on the χ^2 value from the weighted average for $N_f = 2+1+1$ is 1.81. It causes the error to be increased compared to FLAG 21. For the $N_f = 2+1$ average the stretching factor is 1.04. We hope that the differences for $N_f = 2+1+1$ get resolved in the near future and the uncertainty of the average decreases.

Gradient flow scale w_0

For $N_f = 1+1+1+1$, including QED, there is a single calculation, BMW 20 [23] with the result

$$N_f = 1+1+1+1+\text{QED}: \qquad w_0 = 0.17236(70)\ \text{fm} \qquad \text{Ref. [23]}. \tag{500}$$

For $N_f = 2+1+1$ we now have four calculations ETM 21 [12], CalLat 20A [13], MILC 15 [14], and HPQCD 13A [15] entering the FLAG average. The proceedings ETM 20 is superseded by ETM 21. As discussed above in connection with $\sqrt{t_0}$, we assume 100% correlation between the statistical errors of CalLat 20A, MILC 15, and HPQCD 13A.

For $N_f = 2+1$, we have three calculations RBC/UKQCD 14B [20], HotQCD 14 [21], and BMW 12A [22] that enter the FLAG average. These calculations are independent, and no

correlation is used. QCDSF/UKQCD 15B [56] does not contribute to the average, because it is not published.

Performing the weighted and correlated average, we obtain

$$N_f = 2+1+1: \qquad w_0 = 0.17256(103)\ \text{fm} \qquad \text{Refs. [12–15]}, \tag{501}$$
$$N_f = 2+1: \qquad w_0 = 0.17355(92)\ \text{fm} \qquad \text{Refs. [20–22]}. \tag{502}$$

As above, $N_f = 2+1+1$ results of staggered fermions and the twisted-mass result are not well compatible. The resulting stretching factor based on the χ^2 value from the weighted average is 1.67. It causes the error to be slightly increased compared to FLAG 21. For the $N_f = 2+1$ average the stretching factor is 1.23. We hope that the differences for $N_f = 2+1+1$ get resolved in the near future and the uncertainty of the average decreases.

Isospin-breaking and electromagnetic corrections are expected to be small at the level of present uncertainties. This is also confirmed by the explicit computation by BMW 12A. Therefore, we also perform an average over all $N_f > 2+1$ computations and obtain

$$N_f > 2+1: \qquad w_0 = 0.17250(70)\ \text{fm} \qquad \text{Refs. [12–15, 23]}. \tag{503}$$

For the $N_f > 2+1$ average the rescaling factor is 1.45.

Gradient flow scale t_0/w_0

Currently, there is only one calculation of the scale t_0/w_0 available from ETM 21 [12] which forms the FLAG average

$$N_f = 2+1+1: \qquad t_0/w_0 = 0.11969(62)\ \text{fm} \qquad \text{Ref. [12]}. \tag{504}$$

Potential scale r_0

For $N_f = 2+1+1$, there are two determinations of r_0 from ETM 14 [63] and TUMQCD 22 [62], which contribute to the FLAG average and these are uncorrelated.

For $N_f = 2+1$, all but one calculation fulfill all the criteria to enter the FLAG average. HotQCD 14 [21] is essentially an update of HotQCD 11 [60] by enlarging the set of ensembles used in the computation. Therefore, the result from HotQCD 14 supersedes the one from HotQCD 11 and, hence, we only use the former in the average. The computation of χQCD [65] is based on the configurations produced by RBC/UKQCD 10A [24], and we, therefore, assume a 100% correlation between the statistical errors of the two calculations. HPQCD 05B [54] enhances the calculation of Aubin 04 [68] by adding ensembles at a coarser lattice spacing and using the same discretization for the valence fermion. Therefore, we consider the full errors (statistical and systematic) on the results from Aubin 04 and HPQCD 05B to be 100% correlated.

Performing the weighted (and correlated) average, we obtain

$$N_f = 2+1+1: \qquad r_0 = 0.4580(73)\ \text{fm} \qquad \text{Refs. [62, 63]}, \tag{505}$$
$$N_f = 2+1: \qquad r_0 = 0.4701(36)\ \text{fm} \qquad \text{Refs. [21, 24, 54, 65, 68]}. \tag{506}$$

We note that for the $N_f = 2+1+1$ average, the stretching factor based on the χ^2-value from the weighted average is 1.25, while for the $N_f = 2+1$ average it is 1.14.

Potential scale r_1

For $N_f = 2{+}1{+}1$, there are three works that fulfill the criteria to enter the FLAG average, namely TUMQCD 22 [62], HPQCD 13A [15] and HPQCD 11B [52]. They are all based on a varying number of MILC-HISQ ensembles and we therefore assume 100% correlation between the statistical errors. The result from HPQCD 13A supersedes the result from HPQCD 11B (in line with a corresponding statement in HPQCD 13A), hence TUMQCD 22 and HPQCD 13A form the FLAG average.

For $N_f = 2+1$, all the results quoted in Tab. 78 fulfill the FLAG criteria, but not all of them enter the average. The published result from MILC 09 [66] is superseded by the result in the proceedings MILC 10 [61], while MILC 09A [67] is a proceedings contribution and does not enter the average. HPQCD 09B [53] uses HISQ valence quarks instead of asqtad valence quarks as in HPQCD 05B [54]. Therefore, we have RBC/UKQCD 10A [24], MILC 10, HPQCD 09B, HPQCD 05B, and Aubin 04 entering the average. However, since the latter four calculations are based on the aqtad MILC ensembles, we attribute 100% correlation on the statistical error between them and 100% correlation on the systematic error between HPQCD 05B and Aubin 04 as discussed above in connection with r_0.

Performing the weighted and correlated average, we obtain

$$N_f = 2+1+1: \qquad r_1 = 0.3068(37)\ \text{fm} \qquad \text{Refs. [15, 62]}, \tag{507}$$

$$N_f = 2+1: \qquad r_1 = 0.3127(30)\ \text{fm} \qquad \text{Refs. [24, 53, 54, 61, 68]}. \tag{508}$$

We note that for the $N_f = 2+1+1$ average the stretching factor based on the χ^2-value from the weighted average is 1.92, while for the $N_f = 2{+}1$ average it is 1.57. While it is not entirely clear what the reasons are for the discrepancies encoded in these stretching factors, excited-state contaminations are likely to play a role. Also for the potential, states with additional pions will play an increasingly important role at small pion masses and are not easily captured.

The scales M_{p4s} and f_{p4s}

As mentioned in Sec. 11.4.3, these scales have been used only by the MILC and FNAL/MILC collaborations [49–51]. The latest numbers from Ref. [50] are $f_{4ps} = 153.98(11)(^{+2}_{-12})(12)[4]$ MeV and $M_{p4s} = 433.12(14)(^{+17}_{-6})(4)[40]$ MeV and, hence, we have

$$N_f = 2+1+1: \qquad f_{4ps} = 153.98(20)\ \text{MeV} \qquad \text{Ref. [50]}, \tag{509}$$

$$N_f = 2+1+1: \qquad M_{4ps} = 433.12(30)\ \text{MeV} \qquad \text{Ref. [50]}. \tag{510}$$

Dimensionless ratios of scales

We start with the ratio $\sqrt{t_0}/w_0$ for which two $N_f = 2+1+1$ calculations from ETM 21 [12] and HPQCD 13A [15] are available and form the FLAG average

$$N_f = 2+1+1: \qquad \sqrt{t_0}/w_0 = 0.832(6) \qquad \text{Refs. [12, 15]}. \tag{511}$$

Here we found a large stretching factor $s(a_{\min}) = 12.3$ for [12]. It was applied to the uncertainty before performing the weighted average and has a large effect. In fact, in the web-update after FLAG 21 the error was an order of magnitude smaller due to the very small error of ETM 21. This is now compensated by the large stretching factor.

For the ratio r_0/r_1 there is only one $N_f = 2{+}1{+}1$ calculation available from TUMQCD 22 [62], which fulfills the FLAG criteria and therefore forms the FLAG average. For $N_f = 2+1$ there are three calculations from HotQCD 11 [60], RBC/UKQCD 10A [24], and Aubin 04

[68] available. They all fulfill the FLAG criteria and enter the FLAG average of this ratio,

$$N_f = 2+1+1: \qquad r_0/r_1 = 1.4968(69) \qquad \text{Ref. [62]}, \tag{512}$$
$$N_f = 2+1: \qquad r_0/r_1 = 1.5049(74) \qquad \text{Refs. [24, 60, 68]}. \tag{513}$$

We note that for $N_f = 2+1$, the stretching factor based on the χ^2-value from the weighted average is 1.54.

Finally, for the ratio r_1/w_0 there is one computation from HotQCD 14 [21] for $N_f = 2+1+1$, and one from HPQCD 13A [15] for $N_f = 2+1$ fulfilling the FLAG criteria, and, hence, forming the FLAG values

$$N_f = 2+1+1: \qquad r_1/w_0 = 1.789(26) \qquad \text{Ref. [15]}, \tag{514}$$
$$N_f = 2+1: \qquad r_1/w_0 = 1.7797(67) \qquad \text{Ref. [21]}. \tag{515}$$

11.7 Observations and conclusions

Unfortunately the different computations for theory scales reported here are generally not in good agreement within each set of $N_f = 2+1+1$ and $2+1$ flavour content. As a measure we list here the stretching factors above one. We remind the reader that their squares are equal to the χ^2/dof of the weighted averages. Quantitatively, the stretching factors are for $N_f = 2+1$: 1.2 (w_0), 1.1 (r_0), 1.6 (r_1), 1.5 (r_0/r_1). For $N_f = 2+1+1$ the numbers are larger: 1.8 ($\sqrt{t_0}$), 1.7 (w_0) 1.3 (r_0) 1.9 (r_1), and due to differences which exist between present-days twisted-mass QCD results and staggered results. Of course, the limited number of large-scale QCD simulations that are available means that there are only a small number of truly independent determinations of the scales. For example, three out of the five computations entering our average for w_0 are based on the same HISQ rooted staggered fermion configurations and thus their differences are only due to the choice of the physical scale (M_Ω vs. f_π), the valence quark action (Möbius domain-wall valence fermions vs. staggered fermions) employed to compute it and different analysis of continuum limit, etc.

Due to the publication of ETM 21, differences between $N_f = 2+1$ and 2+1+1 QCD are now smaller and (within their errors) in agreement with expectations [72, 73]. The effect of the charm quark is $-0.6(8)\%$ on w_0 and $-1.2(9)\%$ on $\sqrt{t_0}$ as computed from the FLAG averages, while precision studies of the decoupling of charm quarks predicted generic effects of a magnitude of only $\approx 0.2\%$ [72, 73] for low-energy quantities. However, the agreement within errors is due to large stretching factors. Taking just the individual results, they do not agree. The differences are between $N_f = 2+1$ calculations and $2+1+1$ calculations, but one can also interpret them as a difference between staggered fermion simulations and Wilson-type ones. Since the FLAG averages have changed quite a bit due to one more computation entering the averages, we are looking forward to further and more precise results to see whether the numbers hold up over time. In this respect, it is highly desirable for future computations to also publish ratios such as $\sqrt{t_0}/w_0$ for which there are few numbers so far.

Such ratios of gradient flow scales are also of high interest in order to better understand the specific discretization errors of gradient flow observables. So far, systematic studies and information on the different contributions (see Sec. 11.4.2 and Ref. [45]) are missing. A worrying result is, for example, the scale-setting study of Ref. [74] on ratios of scales. The authors find indications that the asymptotic $\sim a^2$ scaling does not set in before $a \approx 0.05$ fm and the $a = 0.04$ fm data has a relevant influence on their continuum extrapolations.

A final word concerns the physics scales that all results depend on. While the mass of the Ω baryon is more popular than the leptonic decay rate of the pion, both have systematics which are difficult to estimate. For the Ω baryon it is the contaminations by excited states and for the decay rates it is the QED effects $\delta f_\pi^{\rm isoQCD}$. The uncertainty in V_{ud} is *not* relevant at this stage, but means that one is relying more on the standard model being an accurate low-energy theory than in the case of the Ω mass. In principle, excited-state effects are controlled by just going to large Euclidean time, but, in practice, this yields errors that are too large. One, therefore, performs fits with a very small number of excitations while theoretically there is a multitude of multi-hadron states that are expected to contribute. For the leptonic decay rate of the pion, the situation is quite reversed, namely, the problematic QED contributions have a well-motivated theory: chiral perturbation theory. The needed combination of low-energy constants is not accessible from experiment but its large-N estimate [28] has been (indirectly) confirmed by the recent computation of $\delta f_\pi^{\rm isoQCD}$ [27]. Unfortunately the same comparison is not so favourable for the leptonic Kaon decay.

References

[1] T. Aoyama et al., *The anomalous magnetic moment of the muon in the Standard Model*, *Phys. Rept.* **887** (2020) 1 [2006.04822].

[2] M. Della Morte, A. Francis, V. Gülpers, G. Herdoíza, G. von Hippel, H. Horch et al., *The hadronic vacuum polarization contribution to the muon $g-2$ from lattice QCD*, *JHEP* **10** (2017) 020 [1705.01775].

[3] G.P. Lepage, *The Analysis of Algorithms for Lattice Field Theory*, in *Theoretical Advanced Study Institute in Elementary Particle Physics*, 6, 1989.

[4] M. Luscher, *Computational Strategies in Lattice QCD*, in *Les Houches Summer School: Session 93: Modern perspectives in lattice QCD: Quantum field theory and high performance computing*, 2, 2010 [1002.4232].

[5] B. Jäger, T.D. Rae, S. Capitani, M. Della Morte, D. Djukanovic, G. von Hippel et al., *A high-statistics study of the nucleon EM form factors, axial charge and quark momentum fraction*, *PoS* **LATTICE2013** (2014) 272 [1311.5804].

[6] S. Capitani, M. Della Morte, G. von Hippel, B. Knippschild and H. Wittig, *Scale setting via the Ω baryon mass*, *PoS* **LATTICE2011** (2011) 145 [1110.6365].

[7] [ALPHA 12] P. Fritzsch, F. Knechtli, B. Leder, M. Marinkovic, S. Schaefer et al., *The strange quark mass and the Λ parameter of two flavor QCD*, *Nucl.Phys.* **B865** (2012) 397 [1205.5380].

[8] [ALPHA 13A] S. Lottini, *Chiral behaviour of the pion decay constant in $N_f = 2$ QCD*, *PoS* **LATTICE2013** (2014) 315 [1311.3081].

[9] R. Sommer, *Scale setting in lattice QCD*, *PoS* **LATTICE2013** (2014) 015 [1401.3270].

[10] M. Creutz, *Monte Carlo Study of Quantized SU(2) Gauge theory*, *Phys. Rev.* **D21** (1980) 2308.

[11] R. Sommer, *A new way to set the energy scale in lattice gauge theories and its applications to the static force and α_s in SU(2) Yang-Mills theory*, *Nucl. Phys.* **B411** (1994) 839 [hep-lat/9310022].

[12] [ETM 21] C. Alexandrou et al., *Ratio of kaon and pion leptonic decay constants with $N_f = 2+1+1$ Wilson-clover twisted-mass fermions*, *Phys. Rev. D* **104** (2021) 074520 [2104.06747].

[13] [CalLat 20A] N. Miller et al., *Scale setting the Möbius domain wall fermion on gradient-flowed HISQ action using the omega baryon mass and the gradient-flow scales t_0 and w_0*, *Phys. Rev. D* **103** (2021) 054511 [2011.12166].

[14] [MILC 15] A. Bazavov et al., *Gradient flow and scale setting on MILC HISQ ensembles*, *Phys. Rev.* **D93** (2016) 094510 [1503.02769].

[15] [HPQCD 13A] R. Dowdall, C. Davies, G. Lepage and C. McNeile, *V_{us} from π and K decay constants in full lattice QCD with physical u, d, s and c quarks*, *Phys.Rev.* **D88** (2013) 074504 [1303.1670].

[16] R. J. Hudspith, M.F.M. Lutz and D. Mohler, *Precise Omega baryons from lattice QCD*, 2404.02769.

[17] [RQCD 22] G. S. Bali, S. Collins, P. Georg, D. Jenkins, P. Korcyl, A. Schäfer et al., *Scale setting and the light baryon spectrum in $N_f = 2 + 1$ QCD with Wilson fermions*, *JHEP* **05** (2023) 035 [2211.03744].

[18] [CLS 21] B. Strassberger et al., *Scale setting for CLS 2+1 simulations*, *PoS* **LATTICE2021** (2022) 135 [2112.06696].

[19] [CLS 16] M. Bruno, T. Korzec and S. Schaefer, *Setting the scale for the CLS 2+1 flavor ensembles*, *Phys. Rev.* **D95** (2017) 074504 [1608.08900].

[20] [RBC/UKQCD 14B] T. Blum et al., *Domain wall QCD with physical quark masses*, *Phys. Rev.* **D93** (2016) 074505 [1411.7017].

[21] [HotQCD 14] A. Bazavov et al., *Equation of state in (2+1)-flavor QCD*, *Phys.Rev.* **D90** (2014) 094503 [1407.6387].

[22] [BMW 12A] S. Borsanyi, S. Dürr, Z. Fodor, C. Hoelbling, S.D. Katz et al., *High-precision scale setting in lattice QCD*, *JHEP* **1209** (2012) 010 [1203.4469].

[23] [BMW 20] Sz. Borsanyi et al., *Leading hadronic contribution to the muon magnetic moment from lattice QCD*, *Nature* **593** (2021) 51 [2002.12347].

[24] [RBC/UKQCD 10A] Y. Aoki et al., *Continuum limit physics from 2+1 flavor domain wall QCD*, *Phys.Rev.* **D83** (2011) 074508 [1011.0892].

[25] [PACS-CS 08] S. Aoki et al., *2+1 flavor lattice QCD toward the physical point*, *Phys. Rev.* **D79** (2009) 034503 [0807.1661].

[26] O. Bar, *Chiral perturbation theory and nucleon–pion-state contaminations in lattice QCD*, *Int. J. Mod. Phys. A* **32** (2017) 1730011 [1705.02806].

[27] M. Di Carlo, D. Giusti, V. Lubicz, G. Martinelli, C. Sachrajda, F. Sanfilippo et al., *Light-meson leptonic decay rates in lattice QCD+QED*, *Phys. Rev. D* **100** (2019) 034514 [1904.08731].

[28] V. Cirigliano and I. Rosell, *$\pi/K \to e\bar{\nu}_e$ branching ratios to $O(e^2p^4)$ in Chiral Perturbation Theory*, *JHEP* **10** (2007) 005 [0707.4464].

[29] B. Ananthanarayan and B. Moussallam, *Four-point correlator constraints on electromagnetic chiral parameters and resonance effective Lagrangians*, *JHEP* **06** (2004) 047 [hep-ph/0405206].

[30] V. Cirigliano and H. Neufeld, *A note on isospin violation in $P_{\ell 2}(\gamma)$ decays*, *Phys.Lett.* **B700** (2011) 7 [1102.0563].

[31] Particle Data Group collaboration, *Review of Particle Physics*, *PTEP* **2020** (2020) 083C01.

[32] M. Lüscher, *Properties and uses of the Wilson flow in lattice QCD*, *JHEP* **08** (2010) 071 [1006.4518], [Erratum: *JHEP* **03** (2014) 092].

[33] C.W. Bernard et al., *The static quark potential in three flavor QCD*, *Phys. Rev.* **D62** (2000) 034503 [hep-lat/0002028].

[34] C. Michael, *Adjoint Sources in Lattice Gauge Theory*, *Nucl. Phys.* **B259** (1985) 58.

[35] M. Lüscher and U. Wolff, *How to Calculate the Elastic Scattering Matrix in Two-dimensional Quantum Field Theories by Numerical Simulation*, *Nucl. Phys.* **B339** (1990) 222.

[36] F. Niedermayer, P. Rufenacht and U. Wenger, *Fixed point gauge actions with fat links: Scaling and glueballs*, *Nucl. Phys. B* **597** (2001) 413 [hep-lat/0007007].

[37] [ALPHA 05A] M. Della Morte, A. Shindler and R. Sommer, *On lattice actions for static quarks*, *JHEP* **08** (2005) 051 [hep-lat/0506008].

[38] M. Donnellan, F. Knechtli, B. Leder and R. Sommer, *Determination of the Static Potential with Dynamical Fermions*, *Nucl. Phys. B* **849** (2011) 45 [1012.3037].

[39] A. Hasenfratz and F. Knechtli, *Flavor symmetry and the static potential with hypercubic blocking*, *Phys.Rev.* **D64** (2001) 034504 [hep-lat/0103029].

[40] M. Lüscher and P. Weisz, *Perturbative analysis of the gradient flow in non-abelian gauge theories*, *JHEP* **02** (2011) 051 [1101.0963].

[41] A. Deuzeman and U. Wenger, *Gradient flow and scale setting for twisted mass fermions*, *PoS* **LATTICE2012** (2012) 162.

[42] [ETM 15A] A. Abdel-Rehim et al., *Simulating QCD at the physical point with $N_f = 2$ Wilson twisted mass fermions at maximal twist*, *Phys. Rev.* **D95** (2015) 094515 [1507.05068].

[43] O. Bär and M. Golterman, *Chiral perturbation theory for gradient flow observables*, *Phys. Rev.* **D89** (2014) 034505 [1312.4999], [Erratum: *Phys. Rev.* **D89** (2014) 099905].

[44] S. Schaefer, *Status and challenges of simulations with dynamical fermions*, *PoS* **LATTICE2012** (2012) 001 [1211.5069].

[45] A. Ramos and S. Sint, *Symanzik improvement of the gradient flow in lattice gauge theories*, *Eur. Phys. J. C* **76** (2016) 15 [1508.05552].

[46] [MILC 13B] A. Bazavov et al., *Symanzik Flow on HISQ Ensembles*, *PoS* **LATTICE2013** (2014) 269 [1311.1474].

[47] A. Cheng, A. Hasenfratz, Y. Liu, G. Petropoulos and D. Schaich, *Improving the continuum limit of gradient flow step scaling*, *JHEP* **05** (2014) 137 [1404.0984].

[48] Z. Fodor, K. Holland, J. Kuti, S. Mondal, D. Nogradi et al., *The lattice gradient flow at tree-level and its improvement*, *JHEP* **1409** (2014) 018 [1406.0827].

[49] [FNAL/MILC 14A] A. Bazavov et al., *Charmed and light pseudoscalar meson decay constants from four-flavor lattice QCD with physical light quarks*, *Phys.Rev.* **D90** (2014) 074509 [1407.3772].

[50] [FNAL/MILC 17] A. Bazavov et al., *B- and D-meson leptonic decay constants from four-flavor lattice QCD*, *Phys. Rev.* **D98** (2018) 074512 [1712.09262].

[51] [MILC 12B] A. Bazavov et al., *Lattice QCD ensembles with four flavors of highly improved staggered quarks*, *Phys.Rev.* **D87** (2013) 054505 [1212.4768].

[52] [HPQCD 11B] R. J. Dowdall et al., *The upsilon spectrum and the determination of the lattice spacing from lattice QCD including charm quarks in the sea*, *Phys.Rev.* **D85** (2012) 054509 [1110.6887].

[53] [HPQCD 09B] C. T. H. Davies, E. Follana, I. Kendall, G.P. Lepage and C. McNeile, *Precise determination of the lattice spacing in full lattice QCD*, *Phys.Rev.* **D81** (2010) 034506 [0910.1229].

[54] [HPQCD 05B] A. Gray et al., *The upsilon spectrum and m_b from full lattice QCD*, *Phys.Rev.* **D72** (2005) 094507 [hep-lat/0507013].

[55] [ETM 20] G. Bergner, P. Dimopoulos, J. Finkenrath, E. Fiorenza, R. Frezzotti, M. Garofalo et al., *Quark masses and decay constants in $N_f = 2+1+1$ isoQCD with Wilson clover twisted mass fermions*, in *37th International Symposium on Lattice Field Theory (Lattice 2019) Wuhan, Hubei, China, June 16-22, 2019*, vol. LATTICE2019, p. 181, 2020, DOI [2001.09116].

[56] [QCDSF/UKQCD 15B] V. .G. Bornyakov et al., *Wilson flow and scale setting from lattice QCD*, 1508.05916.

[57] M. Hayakawa and S. Uno, *QED in finite volume and finite size scaling effect on electromagnetic properties of hadrons*, *Prog. Theor. Phys.* **120** (2008) 413 [0804.2044].

[58] M.F.M. Lutz, Y. Heo and X.-Y. Guo, *Low-energy constants in the chiral Lagrangian with baryon octet and decuplet fields from Lattice QCD data on CLS ensembles*, *Eur. Phys. J. C* **83** (2023) 440 [2301.06837].

[59] V. Bornyakov et al., *Determining the scale in Lattice QCD*, 12, 2015 [1512.05745].

[60] [HotQCD 11] A. Bazavov, T. Bhattacharya, M. Cheng, C. DeTar, H. Ding et al., *The chiral and deconfinement aspects of the QCD transition*, *Phys.Rev.* **D85** (2012) 054503 [1111.1710].

[61] [MILC 10] A. Bazavov et al., *Results for light pseudoscalar mesons*, *PoS* **LAT2010** (2010) 074 [1012.0868].

[62] [TUMQCD 22] N. Brambilla, R.L. Delgado, A.S. Kronfeld, V. Leino, P. Petreczky, S. Steinbeißer et al., *Static energy in (2+1+1)-flavor lattice QCD: Scale setting and charm effects*, *Phys. Rev. D* **107** (2023) 074503 [2206.03156].

[63] [ETM 14] N. Carrasco et al., *Up, down, strange and charm quark masses with N_f = 2+1+1 twisted mass lattice QCD*, *Nucl. Phys.* **B887** (2014) 19 [1403.4504].

[64] T.M.B. Asmussen, R. Höllwieser, F. Knechtli and T. Korzec, *The determination of r_0 and r_1 in Nf=2+1 QCD*, *PoS* **LATTICE2023** (2024) 296 [2312.14726].

[65] [χQCD 14] Y. Yi-Bo et al., *Charm and strange quark masses and f_D_s from overlap fermions*, *Phys. Rev.* **D92** (2015) 034517 [1410.3343].

[66] [MILC 09] A. Bazavov et al., *Full nonperturbative QCD simulations with 2+1 flavors of improved staggered quarks*, *Rev. Mod. Phys.* **82** (2010) 1349 [0903.3598].

[67] [MILC 09A] A. Bazavov et al., *MILC results for light pseudoscalars*, *PoS* **CD09** (2009) 007 [0910.2966].

[68] C. Aubin et al., *Light hadrons with improved staggered quarks: Approaching the continuum limit*, *Phys. Rev.* **D70** (2004) 094505 [hep-lat/0402030].

[69] [MILC 09B] A. Bazavov et al., *Results from the MILC collaboration's SU(3) chiral perturbation theory analysis*, *PoS* **LAT2009** (2009) 079 [0910.3618].

[70] [RBC/Bielefeld 07] M. Cheng et al., *The QCD equation of state with almost physical quark masses*, *Phys. Rev. D* **77** (2008) 014511 [0710.0354].

[71] [HPQCD 03] M. Wingate, C.T. Davies, A. Gray, G.P. Lepage and J. Shigemitsu, *The B_s and D_s decay constants in three flavor lattice QCD*, *Phys.Rev.Lett.* **92** (2004) 162001 [hep-ph/0311130].

[72] [ALPHA 14A] M. Bruno, J. Finkenrath, F. Knechtli, B. Leder and R. Sommer, *Effects of Heavy Sea Quarks at Low Energies*, *Phys. Rev. Lett.* **114** (2015) 102001 [1410.8374].

[73] [ALPHA 17A] F. Knechtli, T. Korzec, B. Leder and G. Moir, *Power corrections from decoupling of the charm quark*, *Phys. Lett. B* **774** (2017) 649 [1706.04982].

[74] [ALPHA 20] R. Höllwieser, F. Knechtli and T. Korzec, *Scale setting for $N_f = 3+1$ QCD*, *Eur. Phys. J. C* **80** (2020) 349 [2002.02866].